Implications of North Atlantic Sea Surface Salinity for Summer Precipitation over the U.S. Midwest: Mechanisms and Predictive Value

LAIFANG LI, RAYMOND W. SCHMITT, AND CAROLINE C. UMMENHOFER

Department of Physical Oceanography, Woods Hole Oceanographic Institution, Woods Hole, Massachusetts

KRISTOPHER B. KARNAUSKAS

Department of Atmospheric and Oceanic Sciences, and Cooperative Institute for Research in Environmental Sciences, University of Colorado Boulder, Boulder, Colorado

(Manuscript received 24 July 2015, in final form 5 February 2016)

ABSTRACT

Moisture originating from the subtropical North Atlantic feeds precipitation throughout the Western Hemisphere. This ocean-to-land moisture transport leaves its imprint on sea surface salinity (SSS), enabling SSS over the subtropical oceans to be used as an indicator of terrestrial precipitation. This study demonstrates that springtime SSS over the northwestern portion of the subtropical North Atlantic significantly correlates with summertime precipitation over the U.S. Midwest. The linkage between springtime SSS and the Midwest summer precipitation is established through ocean-to-land moisture transport followed by a soil moisture feedback over the southern United States. In the spring, high SSS over the northwestern subtropical Atlantic coincides with a local increase in moisture flux divergence. The moisture flux is then directed toward and converges over the southern United States, which experiences increased precipitation and soil moisture. The increased soil moisture influences the regional water cycle both thermodynamically and dynamically, leading to excessive summer precipitation in the Midwest. Thermodynamically, the increased soil moisture tends to moisten the lower troposphere and enhances the meridional humidity gradient north of 36°N. Thus, more moisture will be transported and converged into the Midwest by the climatological low-level wind. Dynamically, the increases in soil moisture over the southern United States enhance the west–east soil moisture gradient eastward of the Rocky Mountains, which can help to intensify the Great Plains low-level jet in the summer, converging more moisture into the Midwest. Owing to these robust physical linkages, the springtime SSS outweighs the leading SST modes in predicting the Midwest summer precipitation and significantly improves rainfall prediction in this region.

1. Introduction

As the planet's largest water reservoir, the global ocean contributes 85% of the evaporation and experiences 77% of the precipitation worldwide (Schmitt 1995; Schanze et al. 2010; Durack 2015). The net difference between evaporation and precipitation is balanced by moisture flux out of the ocean, which will be transported toward the land and enter the terrestrial water cycle via precipitation (Gimeno et al. 2012). Globally, the oceanic moisture flux directly contributes about 35% of

terrestrial precipitation (Bengtsson 2010). Except for mountainous regions or the tropical rain forest where local moisture recycling is a key process, the majority of terrestrial areas require the oceanic moisture to maintain observed precipitation rates (Trenberth 1999; Van der Ent et al. 2010).

Over the globe, the primary net moisture export regions are located over the subtropical oceans (Gimeno et al. 2010; Schanze et al. 2010; Trenberth et al. 2011). Climatologically, these regions serve as moisture sources for terrestrial precipitation and influence a wide sector of the land area, including North America, Eurasia, and the African continent (Trenberth and Guillemot 1995; Trenberth 1999; Gimeno et al. 2010). As climate continues to warm in the future, expansion of the subtropical dry zone is expected to affect

Corresponding author address: Laifang Li, Department of Physical Oceanography, Woods Hole Oceanographic Institution, 266 Woods Hole Rd., Woods Hole, MA 02543.
E-mail: lli@whoi.edu

precipitation on major continents of the world (Seager et al. 2010; Cai et al. 2012; Gimeno et al. 2013). Further, moisture from the subtropical oceans also modulates the intensity of extreme precipitation on land (Chan and Misra 2010).

The evaporation and lateral export of moisture from the subtropical oceans leave an imprint on the sea surface salinity (SSS) field. Resulting from the net removal of freshwater from the ocean surface, the subtropical oceans are characterized by high SSS relative to global mean values (Schmitt 2008). For example, the saltiest region of the open ocean is located in the subtropical North Atlantic, where SSS exceeds 37 psu under the condition that evaporation minus precipitation reaches $1–3 \, m \, yr^{-1}$ (Schmitt 2008; Gordon et al. 2015). The subtropical SSS, in turn, is sensitive to variations in the oceanic water cycle (D'Addezio and Bingham 2014). The long-term salinification of the subtropical oceans provides evidence for an intensification of the global water cycle in a warming climate (Curry et al. 2003; Hosoda et al. 2009; Durack and Wijffels 2010; Helm et al. 2010; Durack et al. 2012; Skliris et al. 2014). Considering the close relationship between subtropical SSS and the oceanic water cycle as well as the connection between oceanic water flux and terrestrial precipitation, we are motivated to explore whether SSS over the subtropical oceans can be an indicator of terrestrial precipitation and thus provide skill for terrestrial rainfall predictions.

Our previous study showed that winter–spring SSS in the northeastern portion of the subtropical North Atlantic can be utilized as a predictor of Sahel monsoon-season precipitation (Li et al. 2016, manuscript submitted to *Sci. Adv.*). High SSS in the spring is associated with increased moisture flux that diverges from the subtropical ocean, converges in the African Sahel, and interacts with local soil moisture, which results in abnormally high precipitation in the monsoon season. This interaction between ocean, land, and atmosphere links subtropical North Atlantic SSS with Sahel precipitation, making springtime SSS a physically meaningful predictor for monsoon-season precipitation in the Sahel. The study by Li et al. (2016, manuscript submitted to *Sci. Adv.*) provides evidence that sustained observations of SSS can improve regional terrestrial climate predictions. With the advances in salinity measurements, including the present generation of satellites that employs L-band radiometry [*Soil Moisture Ocean Salinity* (*SMOS*), *Aquarius*, and *Soil Moisture Active Passive* (*SMAP*)] and the Argo float program, high-resolution salinity observations covering the entire globe are available. However, the mechanisms that link subtropical SSS, ocean–land moisture exchange, and terrestrial

precipitation have yet to be established to provide a physical basis to the prediction.

In the current study, we expand the scope to a broader domain over the entire subtropical North Atlantic. We aim to answer the following: To what extent is SSS over the subtropical North Atlantic related to terrestrial precipitation, and what are the first-order physical processes? To achieve this, we define a set of SSS indices over the subtropical North Atlantic according to the direction of the divergent component of moisture flux (see details in section 2). Using the SSS indices, we first establish statistical relationships between springtime SSS and summer-season terrestrial precipitation. In addition to the relationship between SSS in the northeast part of the subtropical North Atlantic and Sahel precipitation (Li et al. 2016, manuscript submitted to *Sci. Adv.*), we found a significant springtime SSS signal in the northwestern portion of the subtropical basin, which leads summer precipitation in the U.S. Midwest, an important agricultural region vulnerable to floods and drought (Mo and Lettenmaier 2015). Further, by assessing the atmospheric moisture budget and diagnosing soil moisture content anomaly, we notice that the springtime SSS and U.S. Midwest summer precipitation are connected through land–ocean moisture exchange, its influence on soil moisture content, and most importantly the modulation of soil moisture on the key circulation system [i.e., the Great Plains low-level jet (GPLLJ); Higgins et al. 1997; Cook et al. 2008; Weaver and Nigam 2008].

The rest of the manuscript is organized as follows. Section 2 presents the data and methods used in this study, including the definition of regional SSS indices. Section 3 describes the relationship between SSS and terrestrial precipitation. Mechanisms and potential predictability using SSS as a rainfall predictor are discussed in section 4 and section 5, respectively. Section 6 provides a summary of the findings and conclusions.

2. Data and methods

a. Observations

The salinity dataset used in this study is the Met Office (UKMO) EN4 dataset (Good et al. 2013). The salinity profiles are quality controlled and are from observation-based sources, including the World Ocean Database 2005, the global temperature–salinity profile program, and the Argo float data. The salinity data we used in this study are the objectively analyzed data with $1° \times 1°$ spatial resolution

and monthly temporal resolution. The SSS refers to salinity at 5-m depth.

The primary precipitation dataset used in this study is the National Oceanic and Atmospheric Administration (NOAA) Precipitation Reconstruction over Land (PREC/L; $0.5° \times 0.5°$) (Chen et al. 2002). In addition, to analyze the relationship with U.S. summer precipitation, we adopted the NOAA/Climate Prediction Center (CPC) U.S. unified precipitation ($0.25° \times 0.25°$) dataset (Higgins et al. 2000b).

NCEP–NCAR reanalyses ($2.5° \times 2.5°$) datasets (Kalnay et al. 1996) are used to study the atmospheric circulation linking North Atlantic SSS and terrestrial precipitation. In this study, we focus on quantifying the ocean–land moisture flux and the atmospheric moisture budget over the land area. In addition, NOAA/CPC soil moisture content (Fan and van den Dool 2004) is analyzed to study the land surface mechanisms that extend the springtime SSS signal to summer precipitation on land. The CPC soil moisture product is derived from a surface hydrological model forced by atmospheric observations rather than direct soil observations. However, the CPC soil moisture product is the only long-term soil moisture dataset to match the study period. Further, the datasets show high consistency with observations in terms of land surface moisture balance in North America (Van den Dool et al. 2003).

The analysis period is 1950–2009 because the pre-1950 SSS data coverage is relatively sparse, though the North Atlantic is the best sampled ocean (Skliris et al. 2014). The data analyzed in this study are at monthly resolution, and we have removed the linear trends in all data prior to analysis.

b. Definition of North Atlantic SSS indices

We construct a set of subtropical SSS indices. First, we define the subtropical ocean as the area of net divergence of moisture flux away from the local atmospheric column (Fig. 1). Next, the subtropical ocean is further divided into four areas (roughly equivalent to quadrants) according to the orientation of the divergent component of moisture flux. For example, the northwest (NW) quadrant is where the divergent component of moisture flux is directed toward the northwest (Fig. 1). SSS is averaged within the northwest quadrant to define the NW SSS index. The same method is applied to define the northeast (NE), southwest (SW), and southeast (SE) SSS indices (Fig. 1). Since the divergent component of moisture flux indicates a likely destination where subtropical moisture will converge, the SSS indices defined here reflect not only the changes in surface freshwater flux
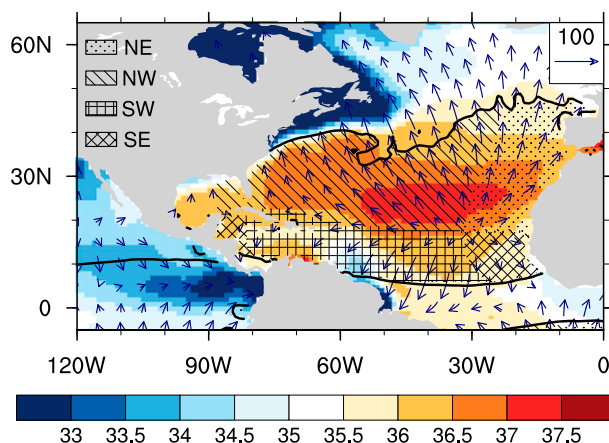

FIG. 1. MAM climatology (1950–2009) of SSS [shaded; units using 1978 practical salinity scale (PSS-78)], moisture flux divergence (thick contours; mm day^{-1}) and the divergent component of moisture flux (vectors; kg m^{-1} s^{-1}) over the North Atlantic. The solid thick contour is the moisture flux divergence = 0 mm day^{-1} isoline, which defines the geographical domain of the subtropical North Atlantic in this study. The domains used to calculate SSS indices in the four quadrants are stippled or hatched.

but also possible geographical areas that will be influenced by the subtropical moisture flux.

Figure 2 shows the interannual variation of springtime [March–May (MAM)] SSS in the four quadrants during 1950–2009. Consistent with the spatial distribution of SSS in the North Atlantic, the baseline SSS in the NW and NE portion of the subtropical basin is higher than in the southern portion of the subtropical oceans (Figs. 1 and 2). In addition, SSS in the four quadrants shows linear trends, with stronger upward trends in the south than in the north (Fig. 2). This SSS trend has been attributed to an intensification of the hydrological cycle in recent decades (Curry et al. 2003; Hosoda et al. 2009; Durack and Wijffels 2010; Helm et al. 2010; Durack et al. 2012; Skliris et al. 2014). In this study, the linear trend in SSS and the other variables are removed so that we may focus on the interannual-to-interdecadal variation of SSS and its relationship with terrestrial precipitation.

At interannual-to-interdecadal time scales, the variations of SSS in the four subdomains are generally independent from one another. Table 1 shows the cross correlation between the four SSS indices. Except for a weakly positive correlation between NW and SW SSS ($R = 0.28$), the other pairwise correlation coefficients are not statistically significant (Table 1). The results suggest that the variation of SSS in the four quadrants is more likely influenced by localized water cycle and
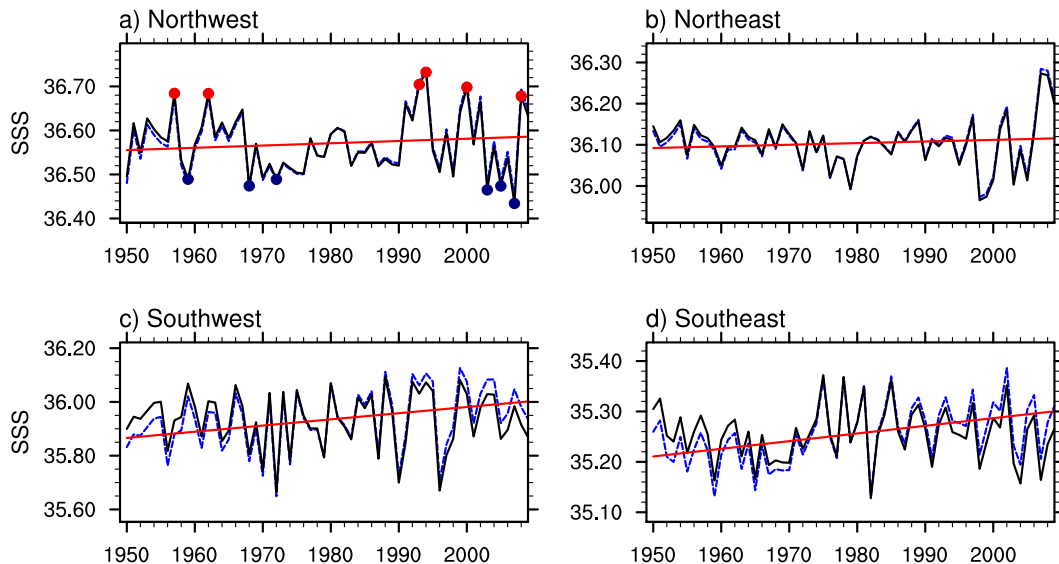
FIG. 2. MAM SSS (dashed blue line) in the four subdomains of the subtropical North Atlantic (shown in Fig. 1): (a) NW, (b) NE, (c) SW, and (d) SE. The solid red lines represent the linear trend of the SSS indices. The solid black lines are the detrended SSS time series. In (a) the red and blue dots mark the high- and low-SSS years, respectively, which are used for composite analysis in the subsequent study.

oceanic processes rather than a response to basinwide climate modes.

c. Thermodynamic and dynamic contributions to atmospheric moisture transport

The atmospheric moisture budget is evaluated to diagnose the processes, either thermodynamic or dynamic, that can provide a physical linkage between terrestrial precipitation and SSS anomalies over the subtropical North Atlantic. According to the budget, moisture fluxes into and out of a local atmospheric column are balanced at a seasonal scale (Brubaker et al. 1993; Trenberth and Guillemot 1995). As a result, precipitation is balanced with evapotranspiration and moisture flux convergence (MFC):

$$P = \text{ET} \underbrace{- \frac{1}{g}\nabla \cdot \int_0^{p_s} q\mathbf{V}\, dp}_{\text{MFC}} + \text{Residual}. \quad (1)$$

In Eq. (1), P is precipitation, ET is evapotranspiration from the land surface to the atmosphere, $-g^{-1}\nabla \cdot \int_0^{p_s} q\mathbf{V}\, dp$ is MFC, with g the gravitational acceleration, q the specific humidity, and $\mathbf{V}$ the horizontal wind velocity vector, and the residual term includes the imbalance of the moisture budget introduced by the increment of reanalysis datasets. To quantify MFC, moisture flux $q\mathbf{V}$ is first calculated at each pressure level and is then integrated from the land surface to the top of the model

level (300 hPa in NCEP–NCAR reanalyses). According to previous studies, the upper limit of the pressure level for the integration does not substantially influence the quantification of MFC because the majority of the moisture is concentrated below 500 hPa (Zhou and Yu 2005; Li et al. 2013; Seager and Henderson 2013).

The MFC can be further decomposed into mass convergence and moisture gradient terms:

$$\underbrace{-\frac{1}{g}\nabla \cdot \int_0^{p_s} q\mathbf{V}\, dp}_{\text{MFC}} = \underbrace{-\frac{1}{g}\int_0^{p_s} q\nabla \cdot \mathbf{V}\, dp}_{\text{mass convergence}} \underbrace{-\frac{1}{g}\int_0^{p_s} \mathbf{V} \cdot \nabla q\, dp}_{\text{moisture gradient}}.$$

$$(2)$$

In addition, thermodynamic and dynamic contributions to the year-to-year variation of MFC can be quantified by decomposing the specific humidity (thermodynamic) and wind (dynamic) in the MFC to a climatology and a deviation from the climatology; that is, $q = q_c + q_a$ and

TABLE 1. Cross correlation between four SSS indices in the subtropical North Atlantic. The correlation coefficients significant at the 0.10 (0.05) level are in italic (boldface) font.

	NW	NE	SW	SE
NW	1	*0.23*	**0.28**	0.19
NE	*0.23*	1	−0.04	0.15
SW	**0.28**	−0.04	1	0.13
SE	0.19	0.15	0.13	1

$\mathbf{V} = \mathbf{V}_c + \mathbf{V}_a$ (Seager et al. 2010; Li et al. 2013). Here, q_c and $\mathbf{V}_c$ are the monthly climatology of specific humidity and wind, respectively, and q_a and $\mathbf{V}_a$ are the deviation from the summertime climatology. The mass convergence and moisture gradient terms in Eq. (2) can thus be decomposed as follows:

$$-\frac{1}{g}\int_0^{p_s} q\nabla \cdot \mathbf{V}\, dp = -\frac{1}{g}\int_0^{p_s} q_c\nabla \cdot \mathbf{V}_c\, dp \underbrace{-\frac{1}{g}\int_0^{p_s} q_a\nabla \cdot \mathbf{V}_c\, dp}_{\text{Thermodynamic}} \underbrace{-\frac{1}{g}\int_0^{p_s} q_c\nabla \cdot \mathbf{V}_a\, dp}_{\text{Dynamic}} -\frac{1}{g}\int_0^{p_s} q_a\nabla \cdot \mathbf{V}_a\, dp \quad \text{and} \quad (3)$$

$$-\frac{1}{g}\int_0^{p_s} \mathbf{V}\cdot\nabla q\, dp = -\frac{1}{g}\int_0^{p_s} \mathbf{V}_c\cdot\nabla q_c\, dp \underbrace{-\frac{1}{g}\int_0^{p_s} \mathbf{V}_c\cdot\nabla q_a\, dp}_{\text{Thermodynamic}} \underbrace{-\frac{1}{g}\int_0^{p_s} \mathbf{V}_a\cdot\nabla q_c\, dp}_{\text{Dynamic}} -\frac{1}{g}\int_0^{p_s} \mathbf{V}_a\cdot\nabla q_a\, dp. \quad (4)$$

On the right-hand side of Eqs. (3) and (4), the first term involves the climatology of specific humidity and wind, which remains constant throughout the analysis period. The second (third) term quantifies the thermodynamic (dynamic) contribution to MFC, in that the wind (specific humidity) is set to the 60-yr climatology. The last term is the covariance of the thermodynamic and dynamic contributions, which is usually an order of magnitude smaller than the thermodynamic and dynamic terms. We thus neglect this term.

d. Random forest regression to predict summer precipitation

To assess the predictability of the summer precipitation using North Atlantic subtropical SSS, we apply the random forest regression algorithm. The random forest regression is a machine-learning algorithm, which takes an ensemble learning approach for prediction. The algorithm is based on the average of decision trees that are built by input training samples (Breiman 2001). The training processes rely on bootstrap aggregating. The algorithm repeatedly subsamples the input data to create regression trees that best fit the relationship between predictors and responses. After training, a prediction based on unseen samples can be made by the ensemble of predictions from the trained regression trees. According to previous studies, the random forest algorithm has advantages in prediction as a result of its ability to avoid overfitting (Breiman 2001).

In this study, we train the random forest regression algorithm with 11 predictors, including SSS, the persistence of regional precipitation, and nine climate indices representing the oceanic and atmospheric modes of variability in the Pacific and Atlantic (Table 2). All climate variables are averaged over MAM to match the SSS predictor. Further, we select the most important rainfall predictors according to the rank of the importance factors. Here, the importance of the ith predictor is quantified as the errors that would be introduced into the prediction if this specific predictor were permutated while the other predictors remained unchanged. The performance of rainfall prediction by the random forest regression is evaluated based on the coefficients of determination: $R^2 = 1 - \mathrm{SS}_{\mathrm{res}}/\mathrm{SS}_{\mathrm{tot}}$ (i.e., the portion of variance explained by the prediction model); $\mathrm{SS}_{\mathrm{tot}} = \sum_{i=1}^{N}(\mathrm{Pr}_i - \overline{\mathrm{Pr}})^2$ is the total variance of observed U.S. Midwest precipitation; and $\mathrm{SS}_{\mathrm{res}} = \sum_{i=1}^{N}[f(\mathbf{X})_i - \mathrm{Pr}_i]^2$ quantifies the sum of precipitation variance unexplained by the prediction, where $f(\mathbf{X})$ is the random forest regression model.

3. Results

a. Relationship between North Atlantic SSS and boreal summer precipitation in the Western Hemisphere

Springtime SSS in the four quadrants of the subtropical North Atlantic is correlated with summer precipitation over land (Fig. 3). According to Fig. 3, the SSS in the four subdomains of the subtropical North Atlantic leads precipitation in different terrestrial areas. Specifically, the NW SSS is most significantly correlated with summer precipitation in the U.S. Midwest, with high SSS corresponding to anomalously high precipitation in the summer (Fig. 3a). The cross correlation between NW SSS and area-averaged U.S. Midwest summer precipitation is 0.42, significant at the 0.01 level. In the NE part of the subtropical North Atlantic, variation of springtime SSS leads summer precipitation in the African Sahel (Fig. 3b). The results are consistent with our previous study showing that the SSS in the NE portion of the subtropical North Atlantic is a useful predictor of monsoon-season precipitation in the African Sahel (Li et al. 2016, manuscript submitted to *Sci. Adv.*). The SSS in the SW and SE of the subtropical basins has weaker correlation with terrestrial precipitation, in comparison with SSS in the northern portion of the subtropical basin (Figs. 3c,d).

TABLE 2. Climate indices used to construct the random forest regression model for U.S. Midwest summer precipitation. The correlation coefficients between climate indices and North Atlantic SSS significant at the 0.10 (0.05) level are in italic (boldface) font.

Index	Description	Correlation with SSS			
		NW	NE	SW	SE
Atlantic multidecadal oscillation (AMO)	SSTA averaged over the North Atlantic (0°–70°N). The linear trend in SSTA has been removed prior to constructing the AMO index.	−0.09	−0.03	−0.11	−0.09
Arctic Oscillation (AO)	The leading EOF mode of sea level pressure variation north of 20°N.	−0.03	0.16	−0.06	−0.17
North Atlantic Oscillation (NAO)	Differences in sea level pressure between Icelandic low and Azores high.	−0.06	0.08	−0.05	−0.20
Niño-3.4	SSTA over the eastern Pacific (5°S–5°N, 170°–120°W).	0.04	−0.11	−0.08	−0.23
Niño-4	SSTA over the central Pacific (5°S–5°N, 160°E–150°W).	−0.03	−0.01	−0.06	−0.24
Pacific decadal oscillation (PDO)	The leading EOF mode of SSTA over the North Pacific (north of 20°N).	−0.14	**−0.29**	0.04	−0.07
Tropical northern Atlantic index (TNA)	SSTA over the tropical Northern Atlantic (5.5°–23.5°N, 57.5°–15°W).	−0.10	−0.03	−0.11	−0.19
Tropical southern Atlantic index (TSA)	SSTA over the tropical Southern Atlantic (20°S–0°, 30°W–10°E).	−0.05	0.03	0.07	−0.13
Western Hemisphere warm pool (WHWP)	The area of over the Atlantic and eastern North Pacific with SST > 28.5°C.	−0.05	−0.12	−0.07	−0.23

In our previous study, the processes linking SSS in the NE portion of the subtropical North Atlantic to Sahel monsoon-season precipitation have been analyzed (Li et al. 2016, manuscript submitted to *Sci. Adv.*). In this study, we primarily focus on the relationship between springtime SSS in the NW subtropical North Atlantic and the U.S. Midwest summer precipitation (Fig. 3a).
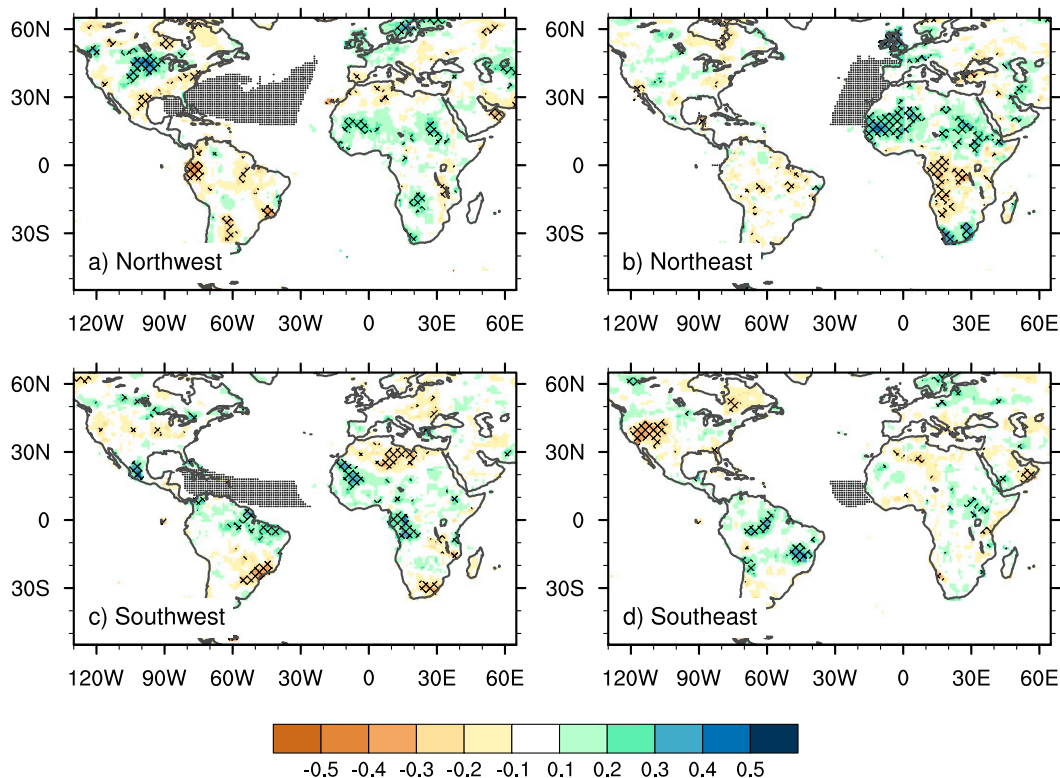

FIG. 3. Correlation between boreal summer (JJA) terrestrial precipitation in the Western Hemisphere (shaded) and springtime North Atlantic SSS indices in the four subdomains of the subtropical basin: (a) NW, (b) NE, (c) SW, and (d) SE. Areas are hatched where the correlation coefficients are significant at the $\alpha = 0.05$ level. The gray-shaded regions in the subtropical North Atlantic are the geographical domains that define the corresponding SSS indices.
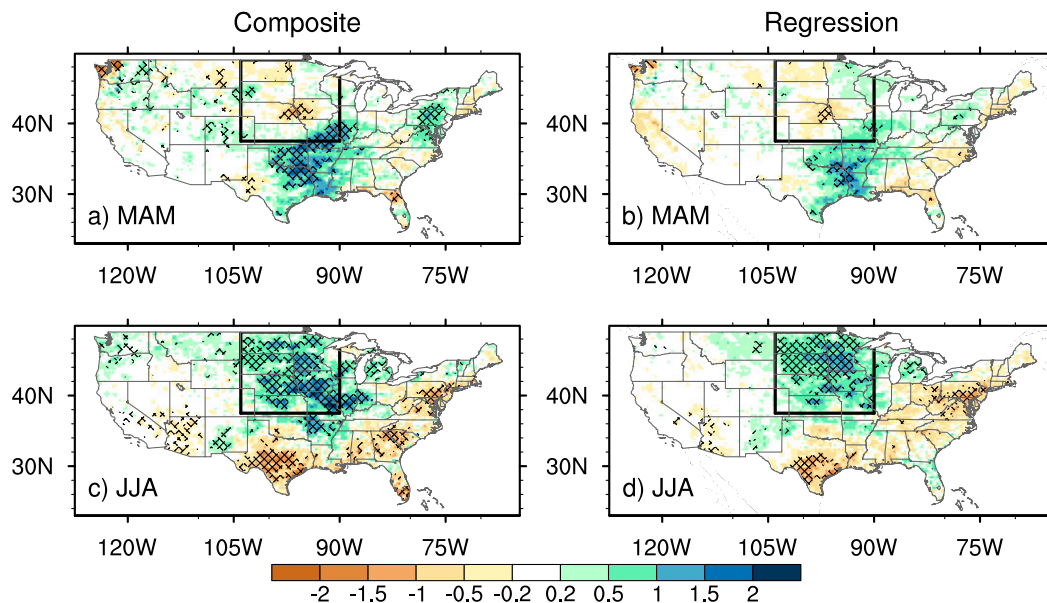
FIG. 4. U.S. precipitation anomalies (shaded; mm day^{-1}) as (a),(c) composite and (b),(d) regressed upon MAM North Atlantic NW SSS index: (top) MAM and (bottom) JJA precipitation. In the composite maps, the precipitation anomalies are the precipitation difference between the top and bottom 10th-percentile SSS cases shown in Fig. 2a. The regions with composite precipitation anomalies or regression coefficients significant at the $\alpha = 0.05$ level are hatched.

To study the evolution of U.S. precipitation from spring (MAM) to summer [June–August (JJA)] corresponding to SSS in the NW subtropical North Atlantic, we applied both composite and linear regression analysis to the NOAA/CPC precipitation dataset. The high and low-SSS cases used for composite analysis are the years with NW SSS ranked among the top and bottom decile of the 1950–2009 records (Fig. 2a). We calculate the differences in precipitation between high and low-SSS years.

For spring precipitation, the most significant signal associated with the NW SSS signal is located over the southern United States (eastward of 100°W), including the eastern part of Texas, Oklahoma, Arkansas, Louisiana, and Mississippi (Figs. 4a,b). The positive precipitation anomalies exceed 1 mm day^{-1}, more than one standard deviation of precipitation in this region (Figs. 4a,b). The positive anomalies in precipitation appear to propagate northward to the U.S. Midwest in the summer (see mechanistic discussion below), leading to 1.5–2 mm day^{-1} above normal precipitation there (Figs. 4c,d). The anomalously high precipitation in the U.S. Midwest is consistent with the SSS–precipitation correlation map shown in Fig. 3a.

Further, the composite and linear regression analyses show qualitatively similar results, especially during the spring season, suggesting that the simultaneous relationship between SSS and precipitation is generally

linear and symmetric (Figs. 4a,b). In the summer, the composite precipitation anomalies are stronger than those in the regression analysis (Figs. 4c,d), likely attributable to nonlinear processes that may amplify the northward-propagating precipitation signal (Blackadar 1957; Holton 1967; Koster et al. 2004; Ting and Wang 2006).

The present analysis shows a robust statistical relationship between the springtime SSS signal in the NW Atlantic and summer precipitation in the U.S. Midwest. Prior to the summer signal, the springtime precipitation anomalies are most significant over the southern United States. Thus, in order to understand the physical linkage between springtime SSS in the NW subtropical North Atlantic and summertime precipitation in the Midwest, the processes linking the springtime SSS and precipitation in the southern United States and how they finally affect summer precipitation in the Midwest must be evaluated.

b. SSS as an indicator of moisture flux from the subtropical North Atlantic

To study the connection between springtime SSS and U.S. precipitation, we analyzed the moisture flux divergence (MFD) and the divergent component of moisture flux (Fig. 5). In the spring, high SSS in the NW subtropical North Atlantic is associated with increased MFD in the atmosphere over the ocean basin (Fig. 5a).
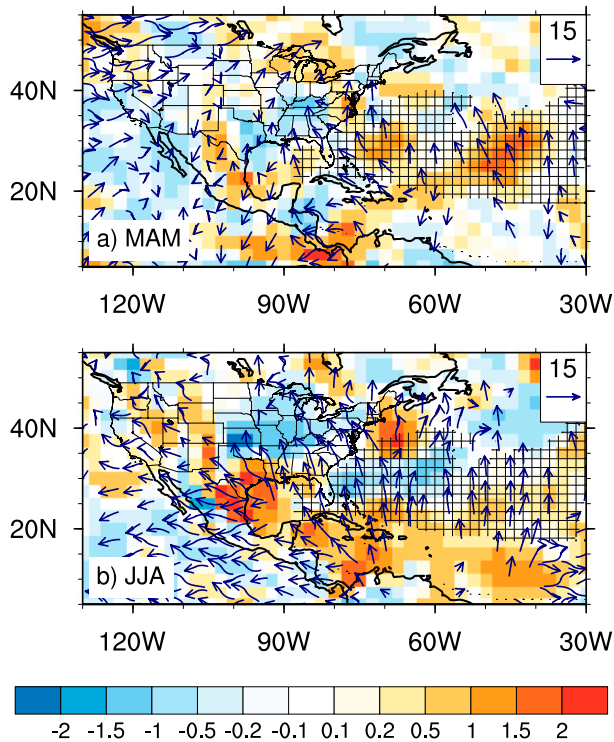
FIG. 5. Anomalies of (a) MAM and (b) JJA moisture flux divergence (shaded; mm day^{-1}) and the divergent component of moisture flux (blue vectors; kg m^{-1} s^{-1}) composite upon the North Atlantic NW SSS index. Only the regions with the divergent component of moisture flux significant at the $\alpha = 0.05$ level by the Hotelling t-squared test are shown. The hatched area represents the geographical domain of the NW subtropical North Atlantic.

According to the MFD differences between the top and bottom decile of NW SSS, there is 1 mm day^{-1} net removal of moisture from the ocean surface in the NW portion of the subtropical basin. According to Yu (2011), over this region, the sea surface moisture flux is a dominant process to generate SSS anomalies, explaining more than 70% of the variance of local SSS variation. Thus, with increased MFD, higher-than-normal SSS is expected as a result of freshwater forcing (Fig. 5a).

Further, we analyzed the divergent component of the moisture flux in order to identify the regions into which these moisture flux will be converged (Chen and Pfaendtner 1993). The orientation of the divergent component of moisture flux suggests that the increased MFD over the subtropical ocean is mainly directed toward the continental United States and converges over the south (Fig. 5a). As a result, the MFC in the South increases by 1 mm day^{-1}, sustaining stronger precipitation in the spring (Figs. 4a,b and 5a). The increased MFC is of similar magnitude to the MFD from the subtropical North Atlantic, as well as the positive precipitation anomalies in the southern United States

(Fig. 4a). The results indicate the importance of moisture from the NW subtropical North Atlantic for affecting the southern United States regional water cycle during the spring season. NW Atlantic SSS, sensitive to the freshwater forcing associated with MFD over the subtropical ocean, thus shows a significant relation with springtime precipitation in the southern United States (Figs. 4a,b).

In the summer, the MFC signal moves northward to the U.S. Midwest, contributing to the above-normal precipitation in this region (Figs. 4c,d and 5b). However, the anomalous MFD over the subtropical North Atlantic weakens, and the northern part of the NW quadrant even shows anomalous MFC (Fig. 5b). Consequently, the primary moisture supply for the higher-than-normal precipitation in the U.S. Midwest comes from the Gulf of Mexico (GOM), where there is high MFD and the divergent component of moisture flux is away from the GOM and toward the U.S. Midwest (Fig. 5b). The moisture source regions identified using the divergent component of moisture flux are consistent with previous studies (Arritt et al. 1997; Higgins et al. 1997; Gimeno et al. 2012). The shift of the moisture export region from the subtropical North Atlantic to the GOM does not contradict our claim that the relationship between North Atlantic subtropical SSS and U.S. Midwest summer precipitation is physically meaningful. Rather it indicates an interaction between springtime moisture flux and land surface processes in the southern United States, whose seasonal evolution influences summer precipitation in the Midwest. In the following sections, we will show that land surface processes extend the springtime NW SSS signals to U.S. Midwest summer precipitation through changes in atmospheric thermodynamics and dynamics associated with the regional water cycle.

c. Thermodynamic and dynamic processes linking North Atlantic SSS variation to U.S. Midwest precipitation

Processes leading to summer precipitation anomalies in the U.S. Midwest during high-SSS years are analyzed from the perspective of the atmospheric moisture balance [Eq. (1)]. On average, the variation of precipitation in this region is mainly modulated by the MFC associated with the monthly mean circulations (Fig. 6). In the past 60 years, the correlation between precipitation and the MFC in summer months is 0.72, indicating that half of the precipitation variance can be explained by the local MFC (Fig. 6a). In high-SSS years, the increase in MFC over the U.S. Midwest is consistent with anomalously high precipitation in the region (Figs. 4c,d and 5b). The close relationship between precipitation and
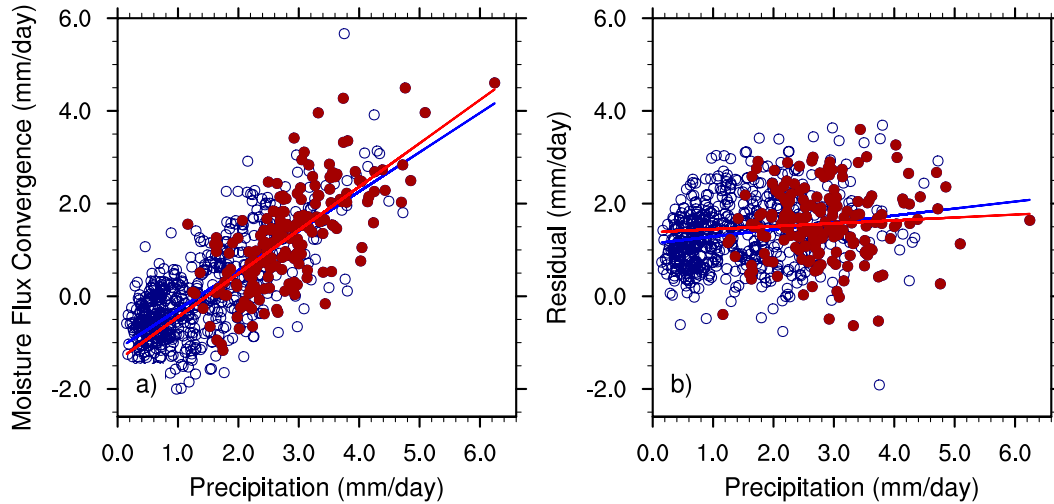
FIG. 6. Relationship between domain-averaged precipitation and (a) the monthly mean component of moisture flux divergence over the Midwest (denoted by the black boxes in Fig. 4) and (b) the residual. The red dots are for JJA and the blue circles are for the other nine months. The red (blue) line is the best least squares linear fit line to the summer season (all-season) sample set.

MFC suggests that analysis of thermodynamic and dynamic processes contributing to MFC changes [Eqs. (3) and (4)] can provide insights to understand the linkage between springtime SSS and U.S. Midwest summer precipitation.

Figure 7 shows the MFC anomalies due to thermodynamic (specific humidity) and dynamic (wind) processes. According to the decomposition method formulated in Eqs. (3) and (4), the increases in MFC and precipitation

in the U.S. Midwest can result from a combination of thermodynamic and dynamic contributions, with dynamic processes playing a more important role (Fig. 7). Specifically, the dynamic contribution is manifest as an increased mass convergence ($-g^{-1} \int_0^{p_s} q_c \nabla \cdot \mathbf{V}_a \, dp$) in the U.S. Midwest (Fig. 7b). The mass convergence term contributes $0.8 \, \text{mm day}^{-1}$ MFC, accounting for approximately 80% of the total MFC anomalies in the U.S. Midwest (Figs. 5b and 7b). Furthermore, the changes in
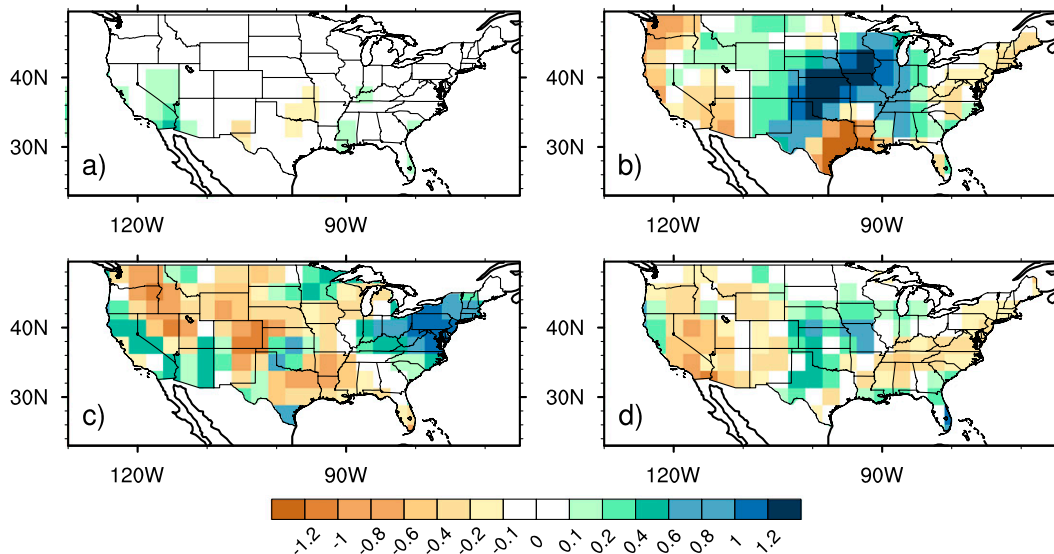

FIG. 7. Thermodynamic and dynamic contributions to moisture flux convergence anomalies (shaded; mm day^{-1}): (a) $-g^{-1} \int_0^{p_s} q_a \nabla \cdot \mathbf{V}_c \, dp$, (b) $-g^{-1} \int_0^{p_s} q_c \nabla \cdot \mathbf{V}_a \, dp$, (c) $-g^{-1} \int_0^{p_s} \mathbf{V}_a \cdot \nabla q_c \, dp$, and (d) $-g^{-1} \int_0^{p_s} \mathbf{V}_c \cdot \nabla q_a \, dp$. The moisture flux convergence anomalies are defined as the differences in MFC between upper and bottom 10th-percentile North Atlantic NW SSS index.

moisture gradient $(-g^{-1}\int_0^{p_s} \mathbf{V}_c \cdot \nabla q_a \, dp)$ result in a $0.2 \, \text{mm day}^{-1}$ MFC anomaly, thermodynamically contributing to excessive precipitation during high-SSS years (Fig. 7d). In contrast, the term $-g^{-1}\int_0^{p_s} q_a \nabla \cdot \mathbf{V}_c \, dp$ does not make a significant contribution to the MFC anomaly (Fig. 7a), while the term $-g^{-1}\int_0^{p_s} \mathbf{V}_a \cdot \nabla q_c \, dp$ tends to reduce MFC and precipitation in the U.S. Midwest (Fig. 7c).

The thermodynamic and dynamic decomposition of MFC attributes the increased summer precipitation during high-SSS years to the enhanced mass convergence and stronger south–north moisture gradient over the Midwest (Figs. 7b,d). The enhanced mass convergence (dynamic contribution), in turn, is linked to an intensification of the GPLLJ during high-SSS years (Fig. 8a). The GPLLJ is characterized as a strong northward airflow that concentrates in the lower troposphere (Fig. 8b). The GPLLJ in the central United States represents the most prominent circulation feature during the spring and summer seasons and is of both hydrological and agricultural importance to the Midwest (Bonner 1968; Higgins et al. 1997; Whiteman et al. 1997; Weaver and Nigam 2008). Figure 8a shows the differences in lower-tropospheric wind (wind averaged between 1000 and 850 hPa) between high- and low-SSS years. In high-SSS years, the meridional wind over the Great Plains (25°–40°N, 95°–105°W) increases by $1 \, \text{m s}^{-1}$, suggesting that the GPLLJ is about 20% stronger than the 60-yr climatology. The intensification of the GPLLJ increases the mass convergence northward of the jet core, leading to excessive MFC over the U.S. Midwest (Arritt et al. 1997; Weaver and Nigam 2008; Weaver et al. 2009a,b; Dirmeyer and Kinter 2010; Cook et al. 2011).

At the same time, the increased south–north moisture gradient is linked to a nonuniform moistening of the lower troposphere over the central United States. The increase in specific humidity is maximal at 36°N, resulting in a stronger south–north moisture gradient northward of 36°N (Fig. 8b). With climatological wind but intensified meridional moisture gradient, more moisture will be imported into the U.S. Midwest along with the northward-moving GPLLJ and hence contribute to a stronger MFC in this region (Fig. 8b).

Overall, the decomposition of MFC suggests that the increases of U.S. Midwest summer precipitation result from combined thermodynamic and dynamics effects, with the dynamic processes playing a more important role. The dynamic processes are linked to an intensification of the GPLLJ, while the thermodynamics are associated with nonuniform increases in the lower-tropospheric humidity over the central United States. The intensification of the GPLLJ and the moistening of the lower troposphere, however, is not caused by
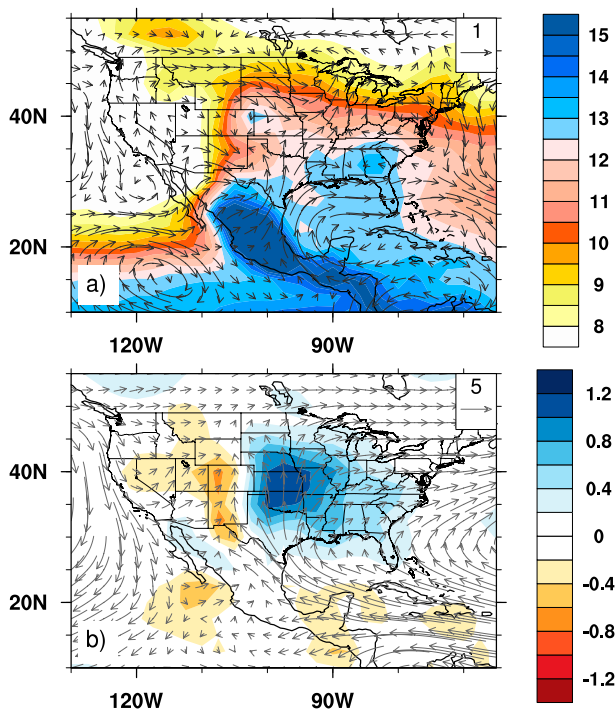

FIG. 8. JJA lower-tropospheric (a) wind anomalies (vectors; m s^{-1}) and (b) moisture content anomalies (shaded; g kg^{-1}) composite on North Atlantic NW SSS index. In (a) the shaded is the climatology of JJA moisture content (g kg^{-1}), and in (b) the vectors are the climatology of lower-tropospheric wind. The lower-tropospheric wind and moisture content are defined as the wind- and specific-humidity-weighted averages between 1000 and 850 hPa, respectively.

springtime SSS in the NW subtropical North Atlantic. Instead, the SSS variation reflects the water cycling in the subtropical North Atlantic and its connection to terrestrial moisture balance, which in turn influences land surface soil moisture content. Through the impact of soil moisture on atmospheric dynamics and thermodynamics, the SSS signal is linked to GPLLJ intensity, lower-tropospheric humidity, and the Midwest precipitation (see section 4 below).

4. Mechanisms: Dual effects of soil moisture

The above analysis shows that high NW Atlantic SSS in spring tends to be followed by above-normal summer precipitation in the U.S. Midwest. The increased precipitation results from both the thermodynamic and dynamic processes that contribute to atmospheric MFC. The summertime MFC in the Midwest follows the seasonal evolution of springtime MFC signal in the South, which can be linked to moisture supplies from the subtropical North Atlantic. The MFD in the North Atlantic leaves its imprint in SSS, yielding a regionally enhanced
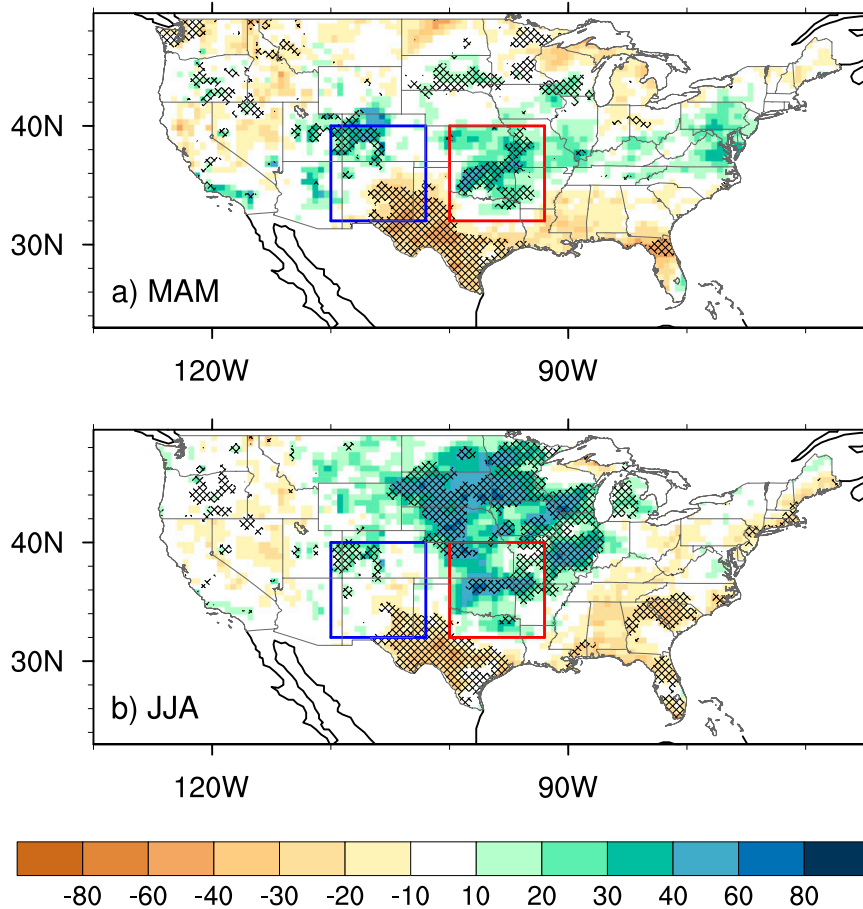
FIG. 9. U.S. soil moisture content anomalies (mm) composite on the North Atlantic NW SSS index: (a) MAM and (b) JJA. The shaded area is the difference between the upper and lower 10th-percentile SSS index. Soil moisture content in the red and blue boxes is used to calculate the west–east soil moisture gradient along the eastern slope of the Rocky Mountains. The hatched areas are the regions where soil moisture content anomaly is significant at the $\alpha = 0.05$ level.

near-surface positive salinity anomaly. However, the connections between springtime NW SSS, moisture supply from the ocean, and summertime atmospheric thermodynamic and dynamic structures in the U.S. Midwest still need to be established.

Given that the SSS signal leads precipitation by a season and the central United States is an area with active land surface coupling, soil moisture is a most likely factor to extend this springtime oceanic signal to the summer season (Koster et al. 2004; Wu et al. 2007; Dirmeyer et al. 2009; Berg et al. 2015). Figure 9 shows the seasonal evolution of soil moisture content anomalies corresponding to years with unusual springtime SSS in the NW subtropical North Atlantic. In the spring, positive anomalies in soil moisture content are found in the southern United States and are largest around 35°N, 97°W (Fig. 9a). This positive soil moisture signal is

located slightly northward of the maximum MFC and precipitation anomalies (Figs. 3a,b, 4a,b, and 9a), re- flecting the response of precipitation to the spatial dis- tribution of soil moisture (Taylor et al. 2011). From spring to summer, the soil moisture anomalies span a wider domain, covering the entire central United States and the Midwest (Fig. 9b). The seasonal migration of soil moisture anomalies can exert dual effects, both thermodynamic and dynamic, on MFC and precipitation in the Midwest.

Thermodynamically, the increased soil moisture content in the central United States favors the partition of radiative energy to latent heat flux and thus increases the evaporation of water vapor from soil to the overlying atmosphere (Meehl and Washington 1988; Delworth and Manabe 1989; Ek and Holtslag 2004). As a result, humidity increases over the regions with elevated soil

moisture content (Delworth and Manabe 1989). This thermodynamic effect of soil moisture can explain the increased lower-tropospheric moisture content in the central United States, which increases the meridional gradient of specific humidity and enhances MFC and precipitation in the Midwest (Figs. 8b and 9b).

In addition, the spatial distribution of soil moisture influences MFC and precipitation through atmospheric dynamics (i.e., the intensity of the GPLLJ). According to Fig. 9b, the increased soil moisture in the central United States enhances the west–east soil moisture gradient along the slope of the Rocky Mountains. By prescribing an increased zonal soil moisture gradient in a numerical model, Fast and McCorcle (1990) showed that the GPLLJ tends to intensify as a result of an increased zonal pressure gradient force (Fast and McCorcle 1990, 1991; Pielke 2001; Frye and Mote 2010).

Such numerical simulation results can be verified by examining the atmospheric reanalysis. We defined the west–east soil moisture gradient as the differences in soil moisture content between the western and eastern boxes shown in Fig. 9. Figure 10 demonstrates the composite of lower-tropospheric wind anomaly upon the soil moisture gradient. Consistent with the numerical simulations, the GPLLJ tends to intensify with a stronger west–east soil moisture gradient. Specifically, the southerly wind along the GPLLJ increases by $1\,\mathrm{m\,s^{-1}}$ in the years with stronger soil moisture gradient (Fig. 10). This magnitude generally agrees with the summertime low-level wind anomalies observed in the composites using the NW SSS index (Figs. 8a and 10). Thus, Fig. 10, combined with previous numerical simulations, suggests that changes in soil moisture gradients can largely explain the dynamic contributions to U.S. Midwest precipitation.

In conclusion, the analysis suggests that soil moisture exerts dual effects on atmospheric thermodynamics and dynamics and thus physically links the springtime SSS signal in the NW subtropical North Atlantic with summer precipitation in the U.S. Midwest. The springtime moisture supply from the subtropical North Atlantic converges into the southern United States, which increases local soil moisture content. At the same time, the increased oceanic moisture flux away from the subtropical oceans increases SSS. Following the seasonal variation of precipitation, MFC, and soil moisture content, the springtime SSS signal is reflected in summer precipitation in the U.S. Midwest. From this perspective, springtime SSS in the NW subtropical North Atlantic can be utilized as a physically meaningful predictor to forecast summer precipitation in the U.S. Midwest.
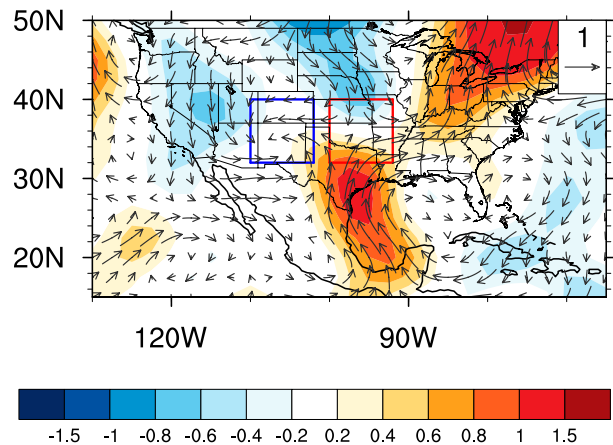

FIG. 10. JJA lower-tropospheric wind (vector; $\mathrm{m\,s^{-1}}$) composite upon soil moisture gradient along the southern slope of the Rockies [defined as the differences between soil moisture content in the western (blue box) and central United States (red box)]. The shaded areas are the meridional wind anomalies. The wind anomalies are calculated as the difference between the upper and lower 10th-percentile soil moisture gradient index.

5. North Atlantic SSS and U.S. Midwest summer rainfall predictability

The predictability of Midwest precipitation using springtime NW SSS is assessed. Prior to applying the NW SSS to prediction models, we test the dependence of the SSS signal on previously identified climate modes (Table 2). These climate modes impact U.S. precipitation by changing the large-scale circulation in which the rainfall-delivering systems develop (Ting and Wang 1997; Higgins et al. 2000a; Barlow et al. 2001; Hu et al. 2011). At the same time, they can affect the processes that generate SSS anomalies (SSSAs) (Mignot and Frankignoul 2003; Reverdin et al. 2007; Yu 2011).

According to our analysis, the SSS in the NW subtropical North Atlantic does not significantly correlate with the leading climate modes that influence summer precipitation in the Midwest (Table 2). For example, the correlation between NW SSS and Niño-3.4 is 0.04 and is −0.06 between the SSS and NAO (Table 2). The insignificant correlations suggest that NW SSS is statistically independent of ENSO and the NAO. Our results are consistent with previous studies that focus on the impact of ENSO and NAO on SSS. The ENSO influence on SSS is mainly over the tropical Pacific and tropical north Indian Ocean but is much less over the North Atlantic (Gouriou and Delcroix 2002; Grunseich et al. 2011). In addition, the NAO mainly influences the SSS during winter seasons and is confined to the midlatitudes (Mignot and Frankignoul 2003). Our analysis combined with these studies suggests that the SSS over the NW subtropical North Atlantic is more influenced by the
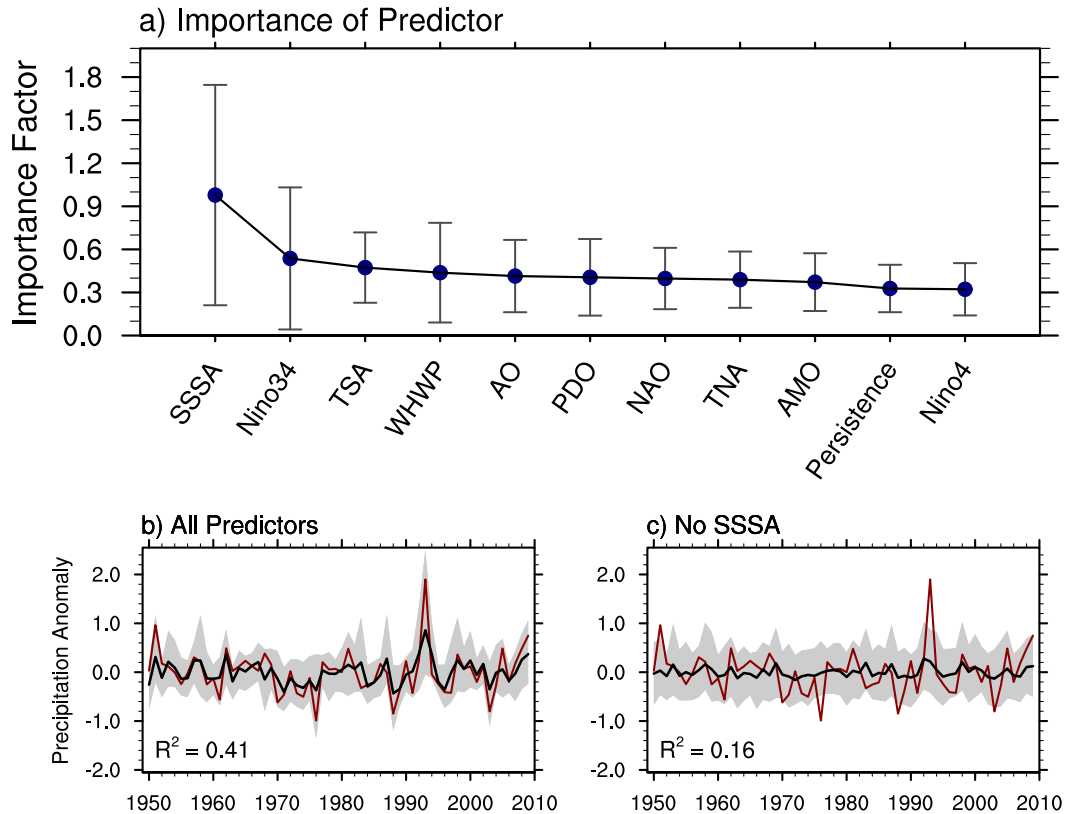
FIG. 11. (a) Importance of 11 predictors used in the random forest prediction model; (b) the random forest regression using top four predictors (NW SSSA, Niño-3.4, TSA, and WHWP) and (c) the prediction without considering the NW SSSA in the North Atlantic. In (b) and (c), the red curves are the observations. The black curves are the predictions by random forest regression, and the gray-shaded areas are the 95% confidence interval of the predictions derived from 1000-iteration random forest regression.

local water cycle (evaporation dominated) than the remote impacts exerted by the climate modes listed in Table 2. This is consistent with the analysis of Yu (2011), who found that SSS variability in the western North Atlantic was largely driven by evaporation minus precipitation ($E - P$).

The relative independence of the NW SSS of climate modes suggests that this SSS signal might provide additional value for the prediction of U.S. Midwest summer precipitation, especially since the SSS signal precedes the precipitation anomalies by a season. Thus, with a better knowledge of springtime SSS over the subtropical North Atlantic, the prediction of U.S. Midwest summer precipitation can be improved.

The predictability of U.S. Midwest precipitation using the salinity predictor is assessed by applying the random forest regression algorithm. According to the 1000 iterations of random forest regression, the NW SSS is ranked as the most important rainfall predictor compared to the other 10 predictors (i.e., the nine climate indices in Table 2 and the persistence of the Midwest

precipitation) (Fig. 11a). Averaged over the 1000 iterations of the regression, the importance factor of NW SSS is 0.98, but it drops to 0.53 for Niño-3.4, the second most important predictor (Fig. 11a). It is noteworthy that the uncertainty range of each predictor's importance factor is relatively large and overlaps with others'. To verify the importance of the SSS predictor, we calculated the probability of SSS being ranked as the top predictor. During the 1000-iteration random forest regression, the probability that SSS is the most important predictor is more than 62%, indicating that the high importance of the SSS predictor is not due to the randomness of the training samples.

Using the top four predictors (NW SSS, Niño-3.4, TSA, and WHWP), we constructed a random forest regression model to predict U.S. Midwest summer precipitation. The prediction was run 1000 times. Each time, 30 samples were randomly drawn for training the algorithm, while the remaining 30 samples were used for prediction. Combining the four predictors, the prediction by the random forest regression explains 41% of
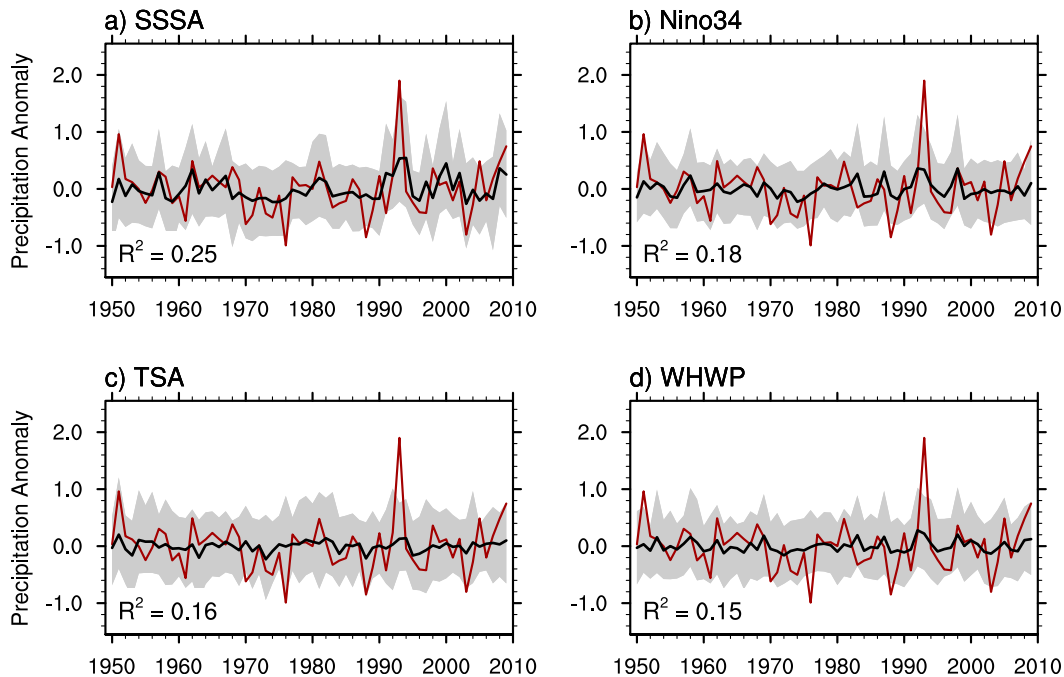
FIG. 12. U.S. Midwest summer precipitation predicted by random forest regression (black curves; mm day^{-1}) considering only the variation of springtime (a) NW subtropical North Atlantic SSSA, (b) Niño-3.4, (c) TSA, and (d) WHWP. The red curves are the observed precipitation anomaly, and the gray-shaded are the 95% confidence interval of the prediction derived from 1000-iteration of random forest regression.

the observed precipitation variance (Fig. 11b). The observed precipitation is within the 95% confidence interval derived from the 1000 iterations of the prediction (Fig. 11b). The prediction without the NW SSS, however, largely underestimates the variability of Midwest precipitation, especially the extremely wet summer in 1993 (Weaver et al. 2009a). At the same time, the R^2 between the observation and prediction decreases to 0.16 (Fig. 11c).

Further, we decomposed the prediction skill into the contribution from each individual predictor. Consistent with the importance factors shown in Fig. 11a, the NW SSS makes the most significant contribution to Midwest rainfall prediction. The variation of NW SSS alone explains 25% of the observed rainfall variance (Fig. 12a). Although the prediction by SSS also underestimates the rainfall variance, it better predicts the extremely wet events than the other predictors (Fig. 12). The predictions by Niño-3.4, TSA, and WHWP further underestimate the interannual variation of U.S. Midwest precipitation (Figs. 12b,d) and thus lower their skill in forecasting the precipitation.

In conclusion, the random forest algorithm demonstrates improvements in Midwest summer rainfall prediction with the knowledge of springtime SSS over the NW subtropical North Atlantic. In addition to the

previously identified ENSO link (Trenberth and Guillemot 1996; Barlow et al. 2001), incorporating NW subtropical North Atlantic SSS into prediction models can thus benefit seasonal forecasting of summer precipitation in the Midwest.

6. Conclusions and discussion

From the perspective of moisture exchange between ocean and land, this study explores the feasibility of terrestrial rainfall prediction using SSS over the subtropical North Atlantic. According to the direction of the divergent component of moisture flux, we divided the subtropical basin into four quadrants and defined a set of SSS indices. We found that springtime SSS over the NW part of the subtropical North Atlantic is significantly correlated with summer precipitation over the U.S. Midwest, suggesting that the NW SSS can be utilized as a predictor of Midwest precipitation.

The linkage between springtime SSS and Midwest summer precipitation is established through the ocean–land moisture transport, land surface–atmospheric coupling, and its impact on atmospheric dynamics and thermodynamics. In the spring, high SSS over the NW portion of the subtropical North Atlantic coincides with an increased MFD away from the local ocean. The flux is

directed toward and converges over the southern United States, supplying extra moisture to this terrestrial domain. The increased moisture supply leads to above-normal springtime precipitation in the southern United States. In the following seasons, the center of positive precipitation anomaly moves northward to the U.S. Midwest.

Analysis of the atmospheric moisture budget shows that the increased Midwest precipitation results from a combination of dynamic and thermodynamic effects on MFC, with the former playing a more important role. The dynamic effect is attributable to an intensification of the GPLLJ resulting from terrestrial moisture gradients, which enhances mass flux convergence over the Midwest. In addition, the thermodynamic effect is manifested by an increase in the lower-tropospheric humidity, which is maximal at 36°N. This spatial distribution of moisture content results in an enhanced meridional moisture gradient north of 36°N, which is favorable for increased MFC over the Midwest.

The dynamic and thermodynamic contributions to MFC might be explained by the dual effects of soil moisture and their influence on the local water cycle. In high-SSS years, the springtime MFC over the southern United States increases local soil moisture content. The soil moisture anomaly interacts with MFC and precipitation in the following seasons and gradually spreads to a wider domain covering the central United States and the Midwest. The increases in soil moisture over the central United States directly moisten the atmospheric boundary layer and thus create a meridional gradient of atmospheric humidity. This effect can explain the diagnosed thermodynamic contributions to MFC over the U.S. Midwest. More importantly, the soil moisture change during high-SSS years increases the west–east soil moisture gradient along the eastern slope of the Rocky Mountains. The increased soil moisture gradient intensifies the GPLLJ, which is favorable for mass convergence at the leading edge of the jet and hence dynamically enhances the MFC over the U.S. Midwest.

Preliminary examination of the North Atlantic spring SSS–Midwest summer rainfall relationship in a number of CMIP5 model runs revealed that 75% of the models showed a similar correlation between high spring SSS and high summer rainfall, though there was variability in the spatial patterns. Full analysis of such model results is beyond the scope of this observational study, but it does suggest that the models do simulate some of the atmospheric processes that transfer moisture from ocean to land.

The close relationship between springtime SSS and U.S. Midwest summer precipitation indicates that salinity variations can provide predictive values for the U.S. Midwest, especially since NW SSS variations are largely independent of the leading climate modes in the Pacific and Atlantic. By applying the random forest regression algorithm to Midwest summer rainfall predictions, we show that NW SSS in the subtropical North Atlantic can generate higher prediction skill than previously identified for ENSO variability. In addition, we ran another set of random forest predictions using both NW SSS and springtime soil moisture in the southern United States (red box in Fig. 9) along with the climate mode indices listed in Table 2. The algorithm ranks salinity as the most important predictor and soil moisture as the second. These results support our proposed mechanism that soil moisture provides a kickoff and delay mechanism that bridges the 3-month time lag between salinity and summer precipitation. The prediction with NW SSS and SST-based predictors explains 41% of the observed precipitation variance. The soil moisture and SST together can explain 27% of the rainfall variance. In contrast, the explained variance decreases to 16% when only the SST modes are used. Thus, our study suggests that NW SSS can provide additional predictive skill for summer precipitation over the U.S. Midwest, an important agricultural region vulnerable to floods and droughts.

REFERENCES

Arritt, R. W., T. D. Rink, M. Segal, D. P. Todey, C. A. Clark, M. J. Mitchell, and K. M. Labas, 1997: The Great Plains low-level jet during the warm season of 1993. *Mon. Wea. Rev.*, **125**, 2176–2192, doi:10.1175/1520-0493(1997)125<2176:TGPLLJ>2.0.CO;2.

Barlow, M., S. Nigam, and E. H. Berbery, 2001: ENSO, Pacific decadal variability, and U.S. summertime precipitation, drought, and streamflow. *J. Climate*, **14**, 2105–2128, doi:10.1175/1520-0442(2001)014<2105:EPDVAU>2.0.CO;2.

Bengtsson, L., 2010: The global atmospheric water cycle. *Environ. Res. Lett.*, **5**, 025202, doi:10.1088/1748-9326/5/2/025202.

Berg, A., and Coauthors, 2015: Interannual coupling between summertime surface temperature and precipitation over land: Processes and implications for climate change. *J. Climate*, **28**, 1308–1328, doi:10.1175/JCLI-D-14-00324.1.

Blackadar, A. K., 1957: Boundary layer wind maxima and their significance for the growth of the nocturnal inversion. *Bull. Amer. Meteor. Soc.*, **38**, 283–290.

Bonner, W. D., 1968: Climatology of the low level jet. *Mon. Wea. Rev.*, **96**, 833–850, doi:10.1175/1520-0493(1968)096<0833: COTLLJ>2.0.CO;2.

Breiman, L., 2001: Random forests. *Mach. Learn.*, **45**, 5–32, doi:10.1023/A:1010933404324.

Brubaker, K. L., D. Entekhabi, and P. S. Eagleson, 1993: Estimation of continental precipitation recycling. *J. Climate*, **6**, 1077–1089, doi:10.1175/1520-0442(1993)006<1077:EOCPR>2.0.CO;2.

Cai, W., T. Cowan, and M. Thatcher, 2012: Rainfall reductions over Southern Hemisphere semi-arid regions: The role of subtropical dry zone expansion. *Sci. Rep.*, **2**, 702, doi:10.1038/srep00702.

Chan, S. C., and V. Misra, 2010: A diagnosis of the 1979–2005 extreme rainfall events in the southeastern United States with isentropic moisture tracing. *Mon. Wea. Rev.*, **138**, 1172–1185, doi:10.1175/2009MWR3083.1.

Chen, M., P. Xie, J. E. Janowiak, and P. A. Arkin, 2002: Global land precipitation: A 50-yr monthly analysis based on gauge observations. *J. Hydrometeor.*, **3**, 249–266, doi:10.1175/ 1525-7541(2002)003<0249:GLPAYM>2.0.CO;2.

Chen, T.-C., and J. Pfaendtner, 1993: On the atmospheric branch of the hydrological cycle. *J. Climate*, **6**, 161–167, doi:10.1175/ 1520-0442(1993)006<0161:OTABOT>2.0.CO;2.

Cook, B. I., R. Seager, and R. L. Miller, 2011: On the causes and dynamics of the early twentieth-century North American pluvial. *J. Climate*, **24**, 5043–5060, doi:10.1175/2011JCLI4201.1.

Cook, K. H., E. K. Vizy, Z. S. Launer, and C. M. Patricola, 2008: Springtime intensification of the Great Plains low-level jet and Midwest precipitation in GCM simulations of the twenty-first century. *J. Climate*, **21**, 6321–6340, doi:10.1175/ 2008JCLI2355.1.

Curry, R., B. Dickson, and I. Yashayaev, 2003: A change in the freshwater balance of the Atlantic Ocean over the past four decades. *Nature*, **426**, 826–829, doi:10.1038/nature02206.

D'Addezio, J. M., and F. M. Bingham, 2014: A subtropical North Atlantic regional atmospheric moisture budget. *J. Geophys. Res. Oceans*, **119**, 8731–8748, doi:10.1002/2014JC010300.

Delworth, T., and S. Manabe, 1989: The influence of soil wetness on near-surface atmospheric variability. *J. Climate*, **2**, 1447–1462, doi:10.1175/1520-0442(1989)002<1447:TIOSWO>2.0.CO;2.

Dirmeyer, P. A., and J. L. Kinter, 2010: Floods over the U.S. Midwest: A regional water cycle perspective. *J. Hydrometeor.*, **11**, 1172–1181, doi:10.1175/2010JHM1196.1.

——, C. A. Schlosser, and K. L. Brubaker, 2009: Precipitation, recycling, and land memory: An integrated analysis. *J. Hydrometeor.*, **10**, 278–288, doi:10.1175/2008JHM1016.1.

Durack, P. J., 2015: Ocean salinity and the global water cycle. *Oceanography*, **28**, 20–31, doi:10.5670/oceanog.2015.03.

——, and S. E. Wijffels, 2010: Fifty-year trends in global ocean salinities and their relationship to broad-scale warming. *J. Climate*, **23**, 4342–4436, doi:10.1175/2010JCLI3377.1.

——, ——, and R. J. Matear, 2012: Ocean salinities reveal strong global water cycle intensification during 1950 to 2000. *Science*, **336**, 455–458, doi:10.1126/science.1212222.

Ek, M. B., and A. A. M. Holtslag, 2004: Influence of soil moisture on boundary layer cloud development. *J. Hydrometeor.*, **5**, 86–99, doi:10.1175/1525-7541(2004)005<0086:IOSMOB>2.0.CO;2.

Fan, Y., and H. van den Dool, 2004: Climate Prediction Center global monthly soil moisture data set at 0.5-degree resolution for 1948 to present. *J. Geophys. Res.*, **109**, D10102, doi:10.1029/ 2003JD004345.

Fast, J. D., and M. D. McCorcle, 1990: A two-dimensional numerical sensitivity study of the Great Plains low-level jet. *Mon. Wea. Rev.*, **118**, 151–163, doi:10.1175/1520-0493(1990)118<0151: ATDNSS>2.0.CO;2.

——, and ——, 1991: The effect of heterogeneous soil moisture on a summer baroclinic circulation in the central United States. *Mon. Wea. Rev.*, **119**, 2140–2167, doi:10.1175/1520-0493(1991)119<2140: TEOHSM>2.0.CO;2.

Frye, J. D., and T. L. Mote, 2010: The synergistic relationship between soil moisture and the low-level jet and its role on the prestorm environment in the southern Great Plains. *J. Appl. Meteor. Climatol.*, **49**, 775–791, doi:10.1175/2009JAMC2146.1.

Gimeno, L., A. Drumond, R. Nieto, R. M. Trigo, and A. Stohl, 2010: On the origin of continental precipitation. *Geophys. Res. Lett.*, **37**, L13804, doi:10.1029/2010GL043712.

——, and Coauthors, 2012: Oceanic and terrestrial sources of continental precipitation. *Rev. Geophys.*, **50**, RG4003, doi:10.1029/2012RG000389.

——, R. Nieto, A. Drumond, R. Castillo, and R. Trigo, 2013: Influence of the intensification of the major oceanic moisture sources on continental precipitation. *Geophys. Res. Lett.*, **40**, 1443–1450, doi:10.1002/grl.50338.

Good, S. A., M. J. Martin, and N. A. Rayner, 2013: EN4: Quality controlled ocean temperature and salinity profiles and monthly objective analyses with uncertainty estimates. *J. Geophys. Res. Oceans*, **118**, 6704–6716, doi:10.1002/2013JC009067.

Gordon, A. L., C. F. Giulivi, J. Busecke, and F. M. Bingham, 2015: Differences among subtropical surface patterns. *Oceanography*, **28**, 32–39, doi:10.5670/oceanog.2015.02.

Gouriou, Y., and T. Delcroix, 2002: Seasonal and ENSO variations of sea surface salinity and temperature in the South Pacific convergence zone during 1976–2000. *J. Geophys. Res.*, **107**, 8011, doi:10.1029/2001JC000830.

Grunseich, G., B. Subrahmanyam, V. S. N. Murty, and B. S. Giese, 2011: Sea surface salinity variability during the Indian Ocean dipole and ENSO events in the tropical Indian Ocean. *J. Geophys. Res.*, **116**, C11013, doi:10.1029/2011JC007456.

Helm, K. P., N. L. Bindoff, and J. A. Church, 2010: Changes in the global hydrological-cycle inferred from ocean salinity. *Geophys. Res. Lett.*, **37**, L18701, doi:10.1029/2010GL044222.

Higgins, R. W., Y. Yao, E. S. Yarosh, J. E. Janowiak, and K. C. Mo, 1997: Influence of the Great Plains low-level jet on summertime precipitation and moisture transport over the central United States. *J. Climate*, **10**, 481–507, doi:10.1175/1520-0442(1997)010<0481: IOTGPL>2.0.CO;2.

——, A. Leetmaa, Y. Xue, and A. Barnston, 2000a: Dominant factors influencing the seasonal predictability of U.S. precipitation and surface air temperature. *J. Climate*, **13**, 3994–4017, doi:10.1175/ 1520-0442(2000)013<3994:DFITSP>2.0.CO;2.

——, W. Shi, E. Yarosh, and R. Joyce, 2000b: Improved United States precipitation quality control system and analysis. NCEP/Climate Prediction Center ATLAS Rep. 7, 40 pp.

Holton, J. R., 1967: The diurnal boundary layer wind oscillation above sloping terrain. *Tellus*, **19A**, 199–205, doi:10.1111/ j.2153-3490.1967.tb01473.x.

Hosoda, S. T., T. Suga, N. Shikama, and K. Mizuno, 2009: Global surface layer salinity change detected by Argo and its implication for hydrological cycle intensification. *J. Oceanogr.*, **65**, 579–596, doi:10.1007/s10872-009-0049-1.

Hu, Q., S. Feng, and R. J. Oglesby, 2011: Variations in North American summer precipitation driven by the Atlantic multidecadal oscillation. *J. Climate*, **24**, 5555–5570, doi:10.1175/ 2011JCLI4060.1.

Kalnay, E., and Coauthors, 1996: The NCEP–NCAR 40-Year Reanalysis Project. *Bull. Amer. Meteor. Soc.*, **77**, 437–471, doi:10.1175/1520-0477(1996)077<0437:TNYRP>2.0.CO;2.

Koster, R. D., and Coauthors, 2004: Regions of strong coupling between soil moisture and precipitation. *Science*, **305**, 1138–1140, doi:10.1126/science.1100217.

Li, L., W. Li, and A. P. Barros, 2013: Atmospheric moisture budget and its regulation of the summer precipitation variability over the southeastern United States. *Climate Dyn.*, **41**, 613–631, doi:10.1007/s00382-013-1697-9.

Meehl, G. A., and W. M. Washington, 1988: A comparison of soil-moisture sensitivity in two global climate models. *J. Atmos. Sci.*, **45**, 1476–1492, doi:10.1175/1520-0469(1988)045<1476: ACOSMS>2.0.CO;2.

Mignot, J., and C. Frankignoul, 2003: On the interannual variability of surface salinity in the Atlantic. *Climate Dyn.*, **20**, 555–565, doi:10.1007/s00382-002-0294-0.

Mo, K. C., and D. P. Lettenmaier, 2015: Heat wave flash droughts in decline. *Geophys. Res. Lett.*, **42**, 2823–2829, doi:10.1002/2015GL064018.

Pielke, R. A., 2001: Influence of the spatial distribution of vegetation and soil on the prediction of cumulus convective rainfall. *Rev. Geophys.*, **39**, 151–177, doi:10.1029/1999RG000072.

Reverdin, G., E. Kestenare, C. Frankignoul, and T. Delcroix, 2007: Surface salinity in the Atlantic Ocean (30°S–50°N). *Prog. Oceanogr.*, **73**, 311–340, doi:10.1016/j.pocean.2006.11.004.

Schanze, J. J., R. W. Schmitt, and L. L. Yu, 2010: The global oceanic freshwater cycle: A state-of-the-art quantification. *J. Mar. Res.*, **68**, 569–595, doi:10.1357/002224010794657164.

Schmitt, R. W., 1995: The ocean component of the global water cycle. *Rev. Geophys.*, **33** (Suppl.), 1395–1409, doi:10.1029/95RG00184.

——, 2008: Salinity and the global water cycle. *Oceanography*, **21**, 12–19, doi:10.5670/oceanog.2008.63.

Seager, R., and N. Henderson, 2013: Diagnostic computation of moisture budgets in the ERA-Interim reanalysis with reference to analysis of CMIP-archived atmospheric model data. *J. Climate*, **26**, 7876–7901, doi:10.1175/JCLI-D-13-00018.1.

——, N. Naik, and G. A. Vecchi, 2010: Thermodynamic and dynamic mechanisms for large-scale changes in the hydrological cycle in response to global warming. *J. Climate*, **23**, 4651–4668, doi:10.1175/2010JCLI3655.1.

Skliris, N., R. Marsh, S. A. Josey, S. A. Good, C. Liu, and R. P. Allan, 2014: Salinity changes in the World Ocean since 1950 in relation to changing surface freshwater fluxes. *Climate Dyn.*, **43**, 709–736, doi:10.1007/s00382-014-2131-7.

Taylor, C. M., A. Gounou, F. Guichard, P. P. Harris, R. J. Ellis, F. Couvreux, and M. D. Kauwe, 2011: Frequency of Sahelian storm initiation enhanced over mesoscale soil-moisture patterns. *Nat. Geosci.*, **4**, 430–433, doi:10.1038/ngeo1173.

Ting, M., and H. Wang, 1997: Summertime U.S. precipitation variability and its relation to Pacific sea surface temperature. *J. Climate*, **10**, 1853–1873, doi:10.1175/1520-0442(1997)010<1853: SUSPVA>2.0.CO;2.

——, and ——, 2006: The role of the North American topography on the maintenance of the Great Plains summer low-level jet. *J. Atmos. Sci.*, **63**, 1056–1068, doi:10.1175/JAS3664.1.

Trenberth, K. E., 1999: Atmospheric moisture recycling: Role of advection and local evaporation. *J. Climate*, **12**, 1368–1381, doi:10.1175/1520-0442(1999)012<1368:AMRROA>2.0.CO;2.

——, and C. J. Guillemot, 1995: Evaluation of the global atmospheric moisture budget as seen from analyses. *J. Climate*, **8**, 2255–2272, doi:10.1175/1520-0442(1995)008<2255:EOTGAM>2.0.CO;2.

——, and ——, 1996: Physical processes involved in the 1988 drought and 1993 floods in North America. *J. Climate*, **9**, 1288–1298, doi:10.1175/1520-0442(1996)009<1288:PPIITD>2.0.CO;2.

——, J. T. Fasullo, and J. Mackaro, 2011: Atmospheric moisture transports from ocean to land and global energy flows in reanalyses. *J. Climate*, **24**, 4907–4924, doi:10.1175/2011JCLI4171.1.

Van den Dool, H., J. Huang, and Y. Fan, 2003: Performance and analysis of the constructed analogue method applied to U.S. soil moisture over 1981–2001. *J. Geophys. Res.*, **108**, 8617, doi:10.1029/2002JD003114.

Van der Ent, R. J., H. H. G. Savenije, B. Schaefli, and S. C. Steele-Dunne, 2010: Origin and fate of atmospheric moisture over continents. *Water Resour. Res.*, **46**, W09525, doi:10.1029/2010WR009127.

Weaver, S. J., and S. Nigam, 2008: Variability of the Great Plains low-level jet: Large-scale circulation context and hydroclimate impacts. *J. Climate*, **21**, 1532–1551, doi:10.1175/2007JCLI1586.1.

——, A. Ruiz-Barradas, and S. Nigam, 2009a: Pentad evolution of the 1988 drought and 1993 flood over the Great Plains: An NARR perspective on the atmospheric and terrestrial water balance. *J. Climate*, **22**, 5366–5384, doi:10.1175/2009JCLI2684.1.

——, S. Schubert, and H. Wang, 2009b: Warm season variations in the low-level circulation and precipitation over the central United States in observations, AMIP simulations, and idealized SST experiments. *J. Climate*, **22**, 5401–5420, doi:10.1175/2009JCLI2984.1.

Whiteman, C. D., X. Bian, and S. Zhong, 1997: Low-level jet climatology from enhanced rawinsonde observations at a site in the southern Great Plains. *J. Appl. Meteor.*, **36**, 1363–1376, doi:10.1175/1520-0450(1997)036<1363:LLJCFE>2.0.CO;2.

Wu, W., R. E. Dickinson, H. Wang, Y. Liu, and M. Shaikh, 2007: Covariabilities of spring soil moisture and summertime United States precipitation in a climate simulation. *Int. J. Climatol.*, **27**, 429–438, doi:10.1002/joc.1419.

Yu, L., 2011: A global relationship between the ocean water cycle and near-surface salinity. *J. Geophys. Res.*, **116**, C10025, doi:10.1029/2010JC006937.

Zhou, T., and R. Yu, 2005: Atmospheric water vapor transport associated with typical anomalous summer rainfall patterns in China. *J. Geophys. Res.*, **110**, D08104, doi:10.1029/2004JD005413.